Orientation Controllable Growth of MoO₃ Nanoflakes: Micro-Raman, Field Emission, and Birefringence Properties

Bin Yan,[†] Zhe Zheng,[†] Jixuan Zhang,[‡] Hao Gong,[‡] Zexiang Shen,[†] Wei Huang,[§] and Ting Yu*,[†]

Division of Physics and Applied Physics, School of Physical and Mathematical Sciences, Nanyang Technological University, Singapore 637371; Department of Materials Science and Engineering, Faculty of Engineering, National University of Singapore, Singapore 117574; and Jiangsu Key Laboratory for Organic Electronics and Information Displays, Nanjing University of Posts and Telecommunications, Nanjing 210046, People's Republic of China

A simple but effective way to control the orientational arrangement of MoO₃ nanoflakes is presented, which offers an opportunity to investigate the anisotropic properties of different crystallographic faces. Their electrical and optical properties are investigated. According to the polarized micro-Raman spectra, oxygen vacancies preferred to be located at the sharp side edges of the lamella, which might play an important role in the catalytic properties of samples. Ascribing to the unique structural geometry and the oxygen-defects-induced reduction of the work function, the electron field emission properties of the samples show that the erect MoO₃ nanoflakes are potential candidates for the cold-cathode-based electronics. Furthermore, strong optical birefringence properties of samples are also first observed.

The effect of dimensionality and geometry on nanomaterials has been extensively studied to meet the demands of miniaturization and better performance for applications. To date, however, controlling the orientation of nanostructure is still a challenge. Recently, substrates with specific crystallographic orientations but having good lattice matching to the nanowires (NWs) were chosen to induce the NWs growth along different orientations.[1−3] In addition, due to the anisotropic properties of samples, various of novel physical properties can be expected.[4−7] Here, we demonstrate a simple but effective way to manipulate the as-grown orthorhombic molybdenum trioxide (α-MoO₃) nanoflakes. Compared with nanowires, nanoflakes have well-defined crystallographic surfaces, which offer opportunities to investigate the anisotropic parameters on nanomaterials.

The crystalline structure of MoO₃ can be visualized as corner-sharing chains of MoO₆ octahedra that share edges with two similar chains to form layers of MoO₃ stoichiometry in the *ac*-plane (inset of Figure 1a). The layers are stacked in a staggered arrangement along the *b*-axis direction and are held together by van der Waals' forces. As one of most important layered oxides, combined with the unique ability of transition-metal ions to change easily their oxidation state and/or arrangement of the coordination polyhedra,[8] it is a good candidate for application on catalyst,[9] sensor,[10] field emission,[11] and photo- and electrochromic devices.[12]

Experimental Methods

In this contribution, the MoO₃ nanoflakes were fabricated by modified hot plate method.[13,14] A Mo foil (15 mm × 15 mm × 0.2 mm) with a purity of 99.9% (Aldrich) was used as the heating target. After being carefully cleaned, it was loaded on the hot plate. A piece of gold-coated-Si (sample 1) or Si (sample 2) was used as the deposition substrate and laid above the foil with a 0.7 mm distance between the foil and substrate surface.[15] Crystalline α-MoO₃ nanoflakes were observed on the silicon substrate after the foil was heated to 450 °C for 4 h. Structural details of the nanoflakes were characterized by X-ray diffraction (XRD) (Bruker D8 with Cu Kα irradiation). The observation of the morphology of the samples was carried out using a JEOL JSM-6700F field-emission scanning electron microscope (FESEM). Transmission electron microscopy (TEM) was performed using a 200 kV field emission gun (JEOL 2010F).

The polarized micro-Raman spectra from individual nanoflakes were carried out with a WITEC CRM200 confocal Raman system using backscattering configuration, where the incident and scattered unit polarization vectors can be mutually rotated in the horizontal microscope plane. Field emission measurements were recorded using parallel-plate configuration in a high-vacuum chamber with a pressure of 3.8×10^{-7} Torr at room temperature.[16] A Keithley 248 high-voltage source unit was used for sourcing the voltage and a Keithely 237 for measuring the current.

Optical polarization microscopy was performed on an Olympus BX 51 microscope equipped with both a polarizer, positioned in the light path before the specimen, and an analyzer, placed in the optical pathway between the objective rear aperture and the observation camera port. In this case, the birefringence properties can be investigated by rotating specimen stage.

Results and Discussion

The XRD patterns of the samples are shown in Figure 1a. All of the reflection peaks can be indexed to α-MoO₃. Figure 1b shows the TEM image of an individual as-grown nanoflake. The amorphous layer can be found on the surface of nanostructure, which might be attributed to the sudden termination of feeding vapor as the evaporation was ceased. The selected area electron diffraction (SAED) pattern of the nanostructure is displayed in the inset of Figure 1b, revealing well-crystallized single crystals. Considering the crystalline structure of MoO₃,

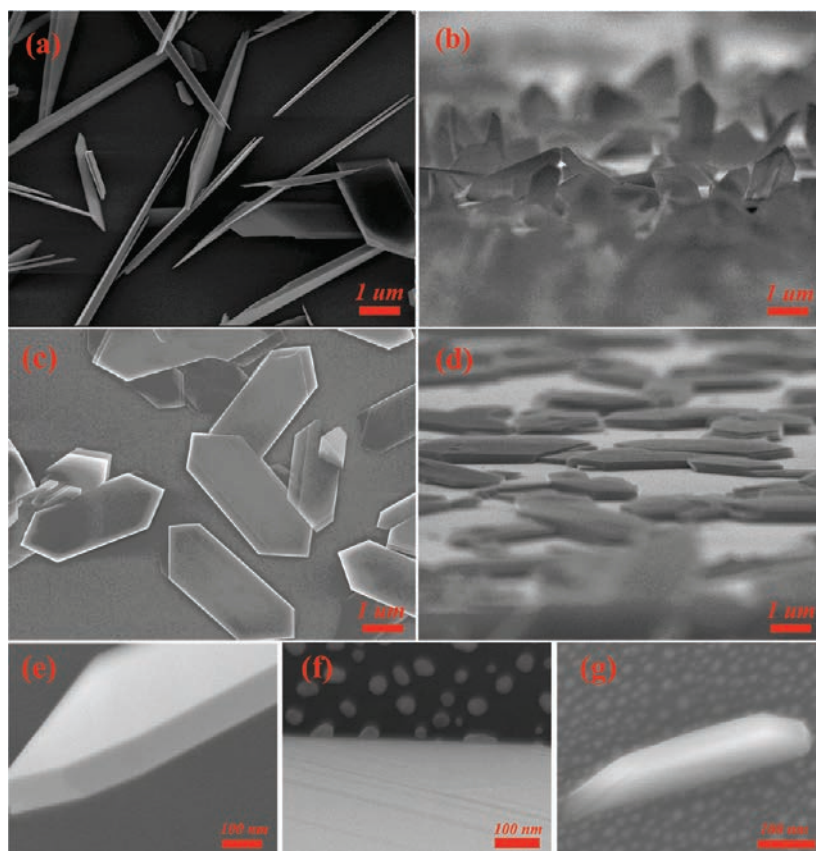* Corresponding author. E-mail: yuting@ntu.edu.sg.
† Nanyang Technological University.
‡ National University of Singapore.
§ Nanjing University of Posts and Telecommunications.
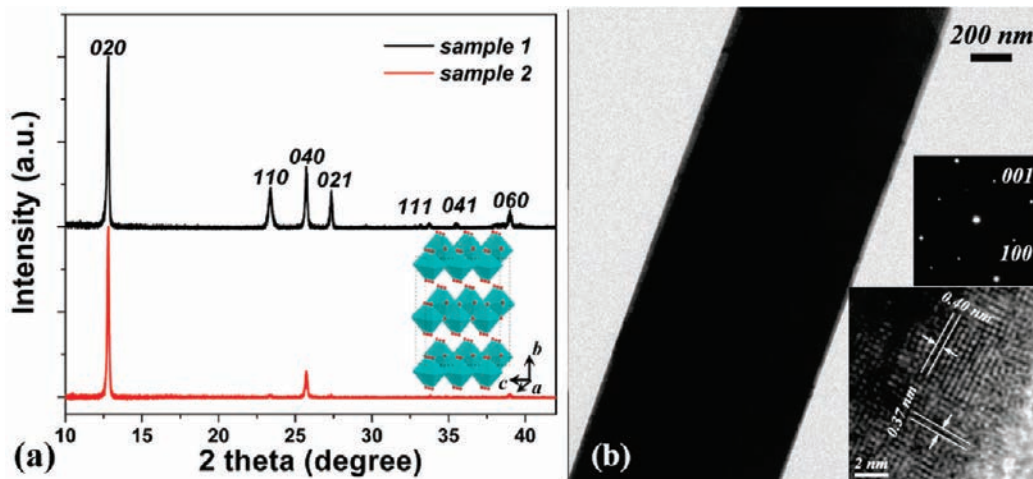
Figure 1. (a) XRD of the as-grown samples. Inset: structural model of MoO_3 with layered structure. (b) TEM image of the MoO_3 nanoflakes and the corresponding electron diffraction patterns.


Figure 2. SEM images of sample 1 and 2: (a, c) top view; (b, d) cross section. High-resolution SEM of sample 1: top edge (e) and bottom (f) of the erect MoO_3 nanoflake. (g) SEM image of sample 1 after being heated for 10 min.

we can see that the thickness of lamella should mainly along $\langle 0k0 \rangle$ direction, which gives rise to a relatively intense diffraction peak of $(0k0)$ plane as shown in Figure 1a. The absence of redundant XRD peaks in sample 2 indicates excellent overall b-axis alignment of these nanoflakes over a large substrate area (the nanoflakes are mainly laid on the substrate). While the appearance of (110) and (021) peaks elucidate the vertically standing on sample 1, which can be further confirmed by SEM images.

As shown in Figure 2, the wirelike features were produced from the top view of sample 1, which is due to the nanoflakes are aligned in a highly dense array approximately perpendicular to the substrate surface. The coverage of the array on the

substrate appears to be quite uniform judging from the SEM images. Cross-section SEM measurements also show that these flakes grow vertically to the substrate surface. While for sample 2, the nanoflakes are just parallel to the substrate. These observations point the importance of gold in mediating the growth of MoO_3 nanoflakes.

The growth of molybdenum trioxide lying on the substrate (sample 2) has been demonstrated previously by vapor–solid (VS) mechanism.[17] To explain the preferable vertical growth of sample 1, high-resolution SEM images are shown in Figure 2, e, f, and g. It is observed that Au particles emerge with nanoflakes at the bottom instead of on the top the structures, even at the very beginning period of growth (Figure 2g), which

Controlled Growth of MoO₃ Nanoflakes

*J. Phys. Chem. C, Vol. 113, No. 47, 2009* **20261**
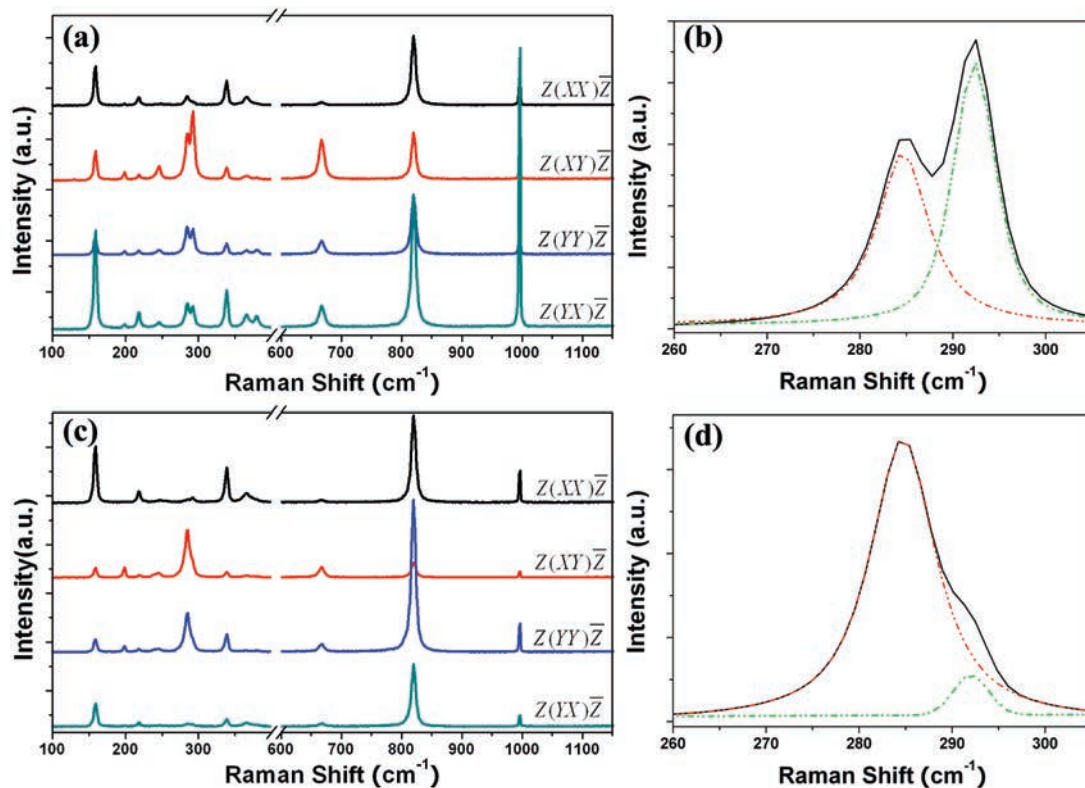
Figure 3. Polarized-Raman spectra of sample 1 (a) and sample 2 (c). The enlarged spectra in $Z(XY)\bar{Z}$ configuration with curve fitting are also shown in panels (b) and (d).
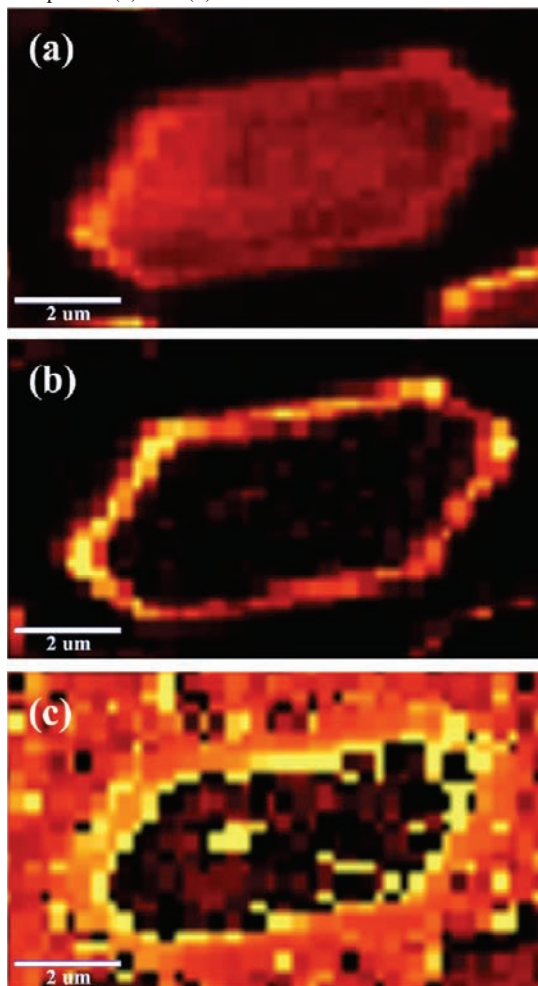
Figure 4. Raman intensity image of the nanoflake constructed by I_{284} (a), I_{293} (b), and I_{293}/I_{284} (c).

is reminiscent that the growth of vertical nanoflake is still governed by the VS mechanism. It is likely that the gold particle strongly lowers the barrier for the incorporation of vapor at the substrate, thus making nanoflakes grow vertically.[18] Besides, the interaction of Au with oxygen facilitates the diffusion of the incoming vapor, which will influence the orientation of the seeds[19,20] and result in the change in arrangement of nanoflakes. From these arguments, it is reasonable to expect that the orientation of single-crystalline MoO₃ nanoflakes can be modified by the existence of Au particles. To further confirm the VS processes, the length and width of more than 50 nanoflakes were measured. As known, the vapor−liquid−solid (VLS) growth tends to produce nanostructures with higher length-to-width ratios than the VS process.[21] The scattered data (not shown here) indicate that the average length-to-width ratio is about 3.25. The value does not change significantly for both samples, which also discloses the same VS growth mechanism.

The unique orientation-ordered geometry of MoO₃ nanoflakes provides a chance to study the physical properties on different crystal faces. The polarized micro-Raman spectra of samples 1 and 2 are presented in Figure 3 under four different scattering configurations. The *Porto notation* was used to indicate the scattering setup in which each spectrum was taken. For example, the symbol $Z(XY)\bar{Z}$ represents that the laser light is incident from the Z direction with the X polarization, while the scattered signal is collected with the Y polarization in the opposite Z direction. The positions of all the Raman peaks observed are in good agreement with those described in the literature,[22−24] while the intensity of the vibration modes varies based on the crystal orientation and the polarized configurations. The observation also confirmed the single-crystalline structure of samples.[25] The Raman peak at 996 cm⁻¹ can be assigned to the asymmetric Mo=O₁ stretching along the *b*-axis direction, while the peak at 819 cm⁻¹ is coming from the symmetric Mo−O₃−Mo stretching
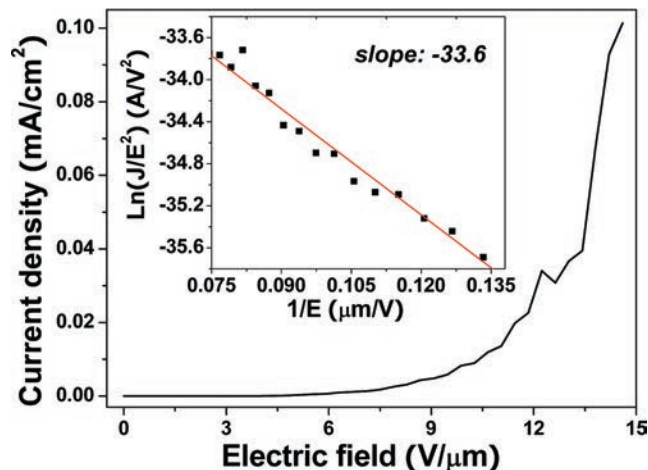
Figure 5. Field emission current−voltage characteristics of sample 1. The inset shows the Fowler−Nordheim (FN) plot.

with the bonding aligning along the *a*-axis.[22] It is observed that the peak strength at 996 cm^{−1} of sample 1 is stronger than sample 2. For the as-grown sample 1 (side edge of MoO_3 nanoflake), *b*-axis direction is perpendicular to the direction of the optical path, which will increase the scattering cross section, especially under $Z(YX)\bar{Z}$ configuration. In contrast, the *a*-axis of sample 2 is parallel to the propagation direction. For the same reason, the signal at 819 cm^{−1} becomes dominant on sample 2. These anisotropic spectra can be used as a benchmark for simple and rapid measurements of nanoflake orientations. Moreover, the two wagging modes of the terminal $Mo=O_1$ groups at 284 cm^{−1} (B_{2g}) and 293 cm^{−1} (B_{3g}) are shown in Figure 3, b and d. For sample 1, the B_{3g} mode is about 2 times stronger than B_{2g} mode. But in the spectra collected from the (*010*) crystalline face (Figure 3d), the B_{3g} mode has only one-seventh of the intensity of the B_{2g} mode. Actually, these wagging modes are both polarized parallel to the *c*-direction, and hence, the changing of intensity ratio reflects symmetry broken introduced by the oxygen defects.[23,26] Far-field Raman mapping was also utilized to further confirm the defects distribution on individual nanoflakes (no analyzer is used in this case). As shown in Figure 4a, the intensity of B_{2g} (centered at 284 cm^{−1}) is uniform over the entire (010) surface plane. In contrast, the B_{3g} band (centered at 293 cm^{−1}), as shown in Figure 4b, exhibits significantly enhancement at the edges of nanoflake. Similarly, the ratio image of I_{293}/I_{284} (Figure 4c) demonstrates clearly that the oxygen defects favor to be at the edge of lamella. As known,

the higher degree of oxygen defects will induce different metal oxidation states, which can promote the catalytic activities. This detailed detection about the distribution of vacancies on different crystalline facets will be helpful for a rational design of more efficient and selective catalysts.

In this work, field emission properties of samples are also investigated. The typical current density−electric field (*J*−*E*) curve of sample 1 is depicted in Figure 5. The turn-on voltage is about 11 V/μm, which is defined as the field to produce a current of 10 μA/cm^{2} for typical operation in flat-panel display. But for sample 2, we found *it is difficult to turn on* the field-induced emission. Using the Fowler−Nordheim (FN) equation for the field emission

$$J = A\left(\frac{\beta^2 E^2}{\varphi}\right)\exp(-B\varphi^{3/2}/\beta E)$$

where $A = 1.56 \times 10^{-10}$ (A V[−2] eV), $B = 6.83 \times 10^9$ (V eV[−3/2] m^{−1}), ϕ is the work function, and β denotes the field enhancement factor, which is related to the emitter geometry, its crystal structure, and spatial distribution of the emitting centers. On the basis of the equation, when $\ln(J/E^2)$ is plotted versus $1/E$, one obtains a straight line with a slope that depends on the work function of material and field enhancement factor β (as shown in the inset of Figure 5). The value of β was obtained to be about 2500, which is also about 4 times larger than the report showing a more random arrangement[27] and comparable to some other II−VI nanomaterials.[28−30] The larger field enhancement factor can be ascribed to the sharp edges of erect nanoflakes. In addition, the oxygen vacancy-type defects may play a critical role in defining the surface properties of sample.[31,32] The modification of surface electronic structure usually alters the Fermi level (work function), and we propose that the oxygen vacancies can reduce work function[31] of the side edges of nanoflakes, which facilitates the electron emission process. As an n-type semiconductor, the oxygen vacancies in MoO_3 act as electron donors. So these donors could shifts the Fermi energy level up, and consequently, the work function (which is defined by the energy difference between Fermi energy level and vacuum level) is lowered. Besides, the removal of the originally negatively charged oxygen ions might lead to the reduction of the Mo ions. It is proposed that the higher concentration of $Mo^{\delta+}$ ($\delta < 6$) species results in a decrease in the work function, which is similar to findings of ref 31. Some further theoretical simulations can be expected. The results also indicate anisotropic
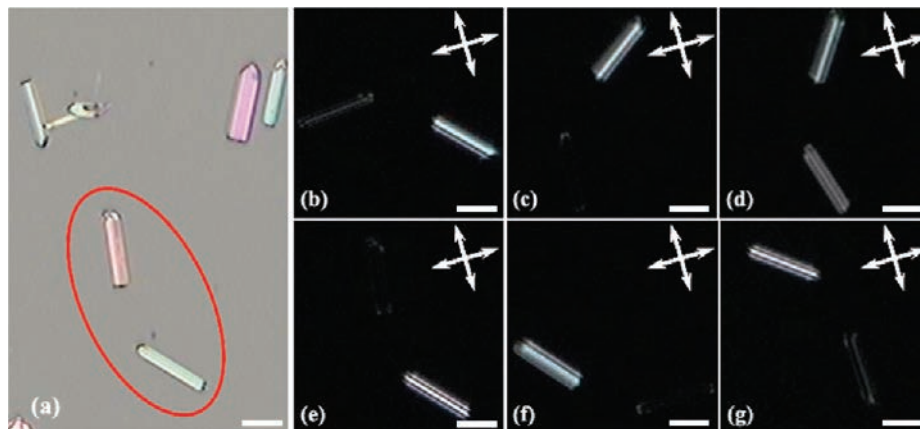
Figure 6. (a) Photomicrograph of samples in normal reflected light. (b−g) Samples observed through cross-polarized optical microscopy with different rotation angles. Scale bar is 5 μm. The top right schemes depict the crossed polarizers (double white arrows).

crystal structure and orientation can affect the performance of nanostructures.

Furthermore, to elucidate the anisotropic optical properties of α-MoO$_3$, the nanoflakes are deposited onto a glass substrate and *first* observed under a polarizing optical microscope using orthogonal linear polarization mode. When drop-cast on substrates from dispersions, the nanoflakes tend to rest on their wide axis. Figure 6a depicts two nanoflakes placed nearly at right angles to each other. The different colors are attributed to the optical interference. Polarized light images of the samples with different rotation angles are illustrated in Figure 6b−g, which shows obvious birefringence due to its anisotropic crystal structure.[33−35] When the incident light is polarizing parallel to only one optical axis, the material appears dark under crossed polarizers, which corresponds to the position of extinction. As the sample rotates away from the position of extinction, splitting of the beam occurs, and the sample appears in the microscope. The nanoflakes are brightest when their spatial axes are about 45° from the polarization angle. Therefore, the contrast between these two nanoflakes can be modified as we rotate the sample. The strong birefringence is attributed to the refractive indices varies with different crystallographic axes ($n_a = 2.29$, $n_b = 1.88$, $n_c = 2.54$)[36] which is constrained by the point group symmetry of the crystal (*Pbnm*-D_{2h}[16]). This distinct phenomena report here makes MoO$_3$ nanoflakes effective building blocks to control the polarization of light in future miniaturized photonics. A more accurate measure of the birefringence can also be expected.

Conclusion

We demonstrate a simple but effective way to control the orientational arrangement of MoO$_3$ nanoflakes, which offers an opportunity to investigate the anisotropic properties of different crystallographic faces. Micro-Raman spectra of the samples revealed that oxygen vacancies prefer to concentrate at the side edges of lamella. Combined with the unique structural geometry, the oxygen-defects-induced reduction of work function on the sharp edges enables erect MoO$_3$ nanoflakes that show promising field emission properties. In addition, strong birefringence properties of the sample were first observed under the polarized light microscope due to their anisotropic crystal structure.

References and Notes

(1) Kuykendall, T.; Pauzauskie, P. J.; Zhang, Y. F.; Goldberger, J.; Sirbuly, D.; Denlinger, J.; Yang, P. D. *Nat. Mater.* **2004**, *3*, 524.

(2) Li, H. W.; Chin, A. H.; Sunkara, M. K. *Adv. Mater.* **2006**, *18*, 216.

(3) Xiong, Q. H.; Chen, G.; Acord, J. D.; Liu, X.; Zengel, J. J.; Gutierrez, H. R.; Redwing, J. M.; Voon, L.; Lassen, B.; Eklund, P. C. *Nano Lett.* **2004**, *4*, 1663.

(4) Pauzauskie, P. J.; Talaga, D.; Seo, K.; Yang, P. D.; Lagugne-Labarthet, F. *J. Am. Chem. Soc.* **2005**, *127*, 17146.

(5) Chen, G.; Wu, J.; Lu, Q. J.; Gutierrez, H. R. H.; Xiong, Q.; Pellen, M. E.; Petko, J. S.; Werner, D. H.; Eklund, P. C. *Nano Lett.* **2008**, *8*, 1341.

(6) Likodimos, V.; Stergiopoulos, T.; Falaras, P.; Kunze, J.; Schmuki, P. *J. Phys. Chem. C* **2008**, *112*, 12687.

(7) Chin, A. H.; Ahn, T. S.; Li, H. W.; Vaddiraju, S.; Bardeen, C. J.; Ning, C. Z.; Sunkara, M. K. *Nano Lett.* **2007**, *7*, 626.

(8) Hu, B.; Mai, L. Q.; Chen, W.; Yang, F. *ACS Nano* **2009**, *3*, 478.

(9) Labanowska, M. *Chemphyschem* **2001**, *2*, 712.

(10) Taurino, A. M.; Forleo, A.; Francioso, L.; Siciliano, P.; Stalder, M.; Nesper, R. *Appl. Phys. Lett.* **2006**, *88*, 152111.

(11) Zhou, J.; Xu, N. S.; Deng, S. Z.; Chen, J.; She, J. C.; Wang, Z. L. *Adv. Mater.* **2003**, *15*, 1835.

(12) Yao, J. N.; Hashimoto, K.; Fujishima, A. *Nature* **1992**, *355*, 624.

(13) Yu, T.; Zhu, Y. W.; Xu, X. J.; Shen, Z. X.; Chen, P.; Lim, C. T.; Thong, J. T. L.; Sow, C. H. *Adv. Mater.* **2005**, *17*, 1595.

(14) Yu, T.; Zhu, Y. W.; Xu, X. J.; Yeong, K. S.; Shen, Z. X.; Chen, P.; Lim, C. T.; Thong, J. T. L.; Sow, C. H. *Small* **2006**, *2*, 80.

(15) Yan, B.; Liao, L.; You, Y. M.; Xu, X. J.; Zheng, Z.; Shen, Z. X.; Ma, J.; Tong, L. M.; Yu, T. *Adv. Mater.* **2009**, *21*, 2436.

(16) Zhu, Y. W.; Yu, T.; Sow, C. H.; Liu, Y. J.; Wee, A. T. S.; Xu, X. J.; Lim, C. T.; Thong, J. T. L. *Appl. Phys. Lett.* **2005**, *87*, 023103.

(17) Zeng, H. C.; Sheu, C. W.; Hia, H. C. *Chem. Mater.* **1998**, *10*, 974.

(18) Velazquez, J. M.; Banerjee, S. *Small* **2009**, *5*, 1025.

(19) Biener, M. M.; Friend, C. M. *Surf. Sci.* **2004**, *559*, L173.

(20) Song, Z.; Cai, T. H.; Chang, Z. P.; Liu, G.; Rodriguez, J. A.; Hrbek, J. *J. Am. Chem. Soc.* **2003**, *125*, 8059.

(21) Lan, Y. C.; Crimp, M. A.; Zhang, J. M. *J. Cryst. Growth* **2006**, *290*, 585.

(22) Liu, D.; Lei, W. W.; Hao, J.; Liu, D. D.; Liu, B. B.; Wang, X.; Chen, X. H.; Cui, Q. L.; Zou, G. T.; Liu, J.; Jiang, S. *J. Appl. Phys.* **2009**, *105*, 023513.

(23) Dieterle, M.; Weinberg, G.; Mestl, G. *Phys. Chem. Chem. Phys.* **2002**, *4*, 812.

(24) Mestl, G.; Srinivasan, T. K. K. *Catal. Rev.-Sci. Eng.* **1998**, *40*, 451.

(25) Zheng, Z.; Yan, B.; Zhang, J.; You, Y.; Lim, C. T.; Shen, Z.; Yu, T. *Adv. Mater.* **2008**, *20*, 352.

(26) Mestl, G.; Srinivasan, T. K. K.; Knozinger, H. *Langmuir* **1995**, *11*, 3795.

(27) Li, Y. B.; Bando, Y.; Golberg, D.; Kurashima, K. *Appl. Phys. Lett.* **2002**, *81*, 5048.

(28) Fang, X.; Bando, Y.; Gautam, U. K.; Ye, C.; Golberg, D. *J. Mater. Chem.* **2008**, *18*, 509.

(29) Fang, X. S.; Bando, Y.; Shen, G. Z.; Ye, C. H.; Gautam, U. K.; Costa, P. M. F. J.; Zhi, C. Y.; Tang, C. C.; Golberg, D. *Adv. Mater.* **2007**, *19*, 2593.

(30) Fang, X. S.; Gautam, U. K.; Bando, Y.; Golberg, D. *J. Mater. Sci. Technol.* **2008**, *24*, 597.

(31) Li, Z. Y.; Wu, Q. H. *J. Mater. Sci.: Mater. Electron.* **2008**, *19*, S366.

(32) Yan, B.; Tao, J. G.; Pang, C.; Zheng, Z.; Shen, Z. X.; Huan, C. H. A.; Yu, T. *Langmuir* **2008**, *24*, 10569.

(33) Sigman, M. B.; Korgel, B. A. *J. Am. Chem. Soc.* **2005**, *127*, 10089.

(34) Biette, L.; Carn, F.; Maugey, M.; Achard, M. F.; Maquet, T.; Steunou, N.; Livage, T.; Serier, H.; Backov, R. *Adv. Mater.* **2005**, *17*, 2970.

(35) Leroy, C. M.; Achard, M. F.; Babot, O.; Steunou, N.; Masse, P.; Livage, J.; Binet, L.; Brun, N.; Backov, R. *Chem. Mater.* **2007**, *19*, 3988.

(36) Deb, S. K. *Proc. R. Soc. London A* **1968**, *304*, 211.